doi:10.3772/j.issn.1006-6748.2019.03.003

A local high-resolution deformation model of soft tissue based on element-free Galerkin method①

Zhang Xiaorui(张小瑞)②[*,**], Yu Xuefeng[*], Sun Wei[**], Zhu Lifeng[***], Liu Jia[**]

([*] Jiangsu Engineering Center of Network Monitoring, Nanjing University of Information Science & Technology, Nanjing 210044, P. R. China)

([**] Jiangsu Collaborative Innovation Center of Atmospheric Environment and Equipment Technology (CICAEET), Nanjing University of Information Science & Technology, Nanjing 210044, P. R. China)

([***] School of Instrument Science and Engineering, Southeast University, Nanjing 210096, P. R. China)

Abstract

In order to solve the problem that the existing meshless models are of high computational complexity and are difficult to express the biomechanical characteristics of real soft tissue, a local high-resolution deformation model of soft tissue based on element-free Galerkin method is proposed. The proposed model applies an element-free Galerkin method to establish the model, and integrates Kelvin viscoelastic model and adjustment function to simulate nonlinear viscoelasticity of soft tissue. Meanwhile, a local high-resolution algorithm is applied to sample and render the deformed region of the model to reduce the computational complexity. To verify the effectiveness of the model, liver and brain tumor deformation simulation experiments are carried out. The experimental results show that compared with the existing meshless models, the proposed model well reflects the biomechanical characteristics of soft tissue, and is of high authenticity, which can provide better visual feedback to users while reducing computational cost.

Key words: meshless model, Kelvin model, local high-resolution, virtual surgery, soft tissue deformation

0 Introduction

The traditional surgical training usually utilizes animal and human remains, which not only wastes manpower and materials, but also may involve ethical issues. Therefore, researchers introduce virtual surgery to improve surgical training effect with new technology instead of traditional surgical training[1-3]. In the early years, the geometric model is often used to directly control the data points or curves on the object surface to simulate the soft tissue deformation, which has high computational efficiency and robustness, but its visual authenticity and simulation accuracy are inferior[4]. In order to overcome these defects, researchers began to use various physical models for soft tissue deformation simulation. At present, the commonly used physical models include mass-spring model, finite element model and meshless model.

The structure and calculation of the mass-spring model are simple, but its precision is low and the model is unstable[5-7]. The finite element model can accurately describe a series of material behaviors with high simulation accuracy. However, due to the introduction of a large number of material parameters, it is difficult to change the topological structure in the simulation process and the computational complexity is high[8-10].

Compared with former models, the meshless model builds virtual soft tissue based on discrete points, which does not need to maintain topological information between the data points. As a result, complex topological structure problems in mesh model like inherent pathological mesh, mesh distortion and topology reconstruction can be avoided. At the same time, discrete points are evenly or randomly distributed in the interior and boundary, which has strong adaptability[11-14], therefore, more attention is given to meshless model by researchers in recent years. However, the calculation cost of meshless model is high, and it still needs to be strengthened in reflecting biomechanical features of soft

① Supported by the National Natural Science Foundation of China (No. 61502240, 61502096, 61304205, 61773219) and Natural Science Foundation of Jiangsu Province (No. BK20141002, BK20150634).

② To whom correspondence should be addressed. E-mail: zxr365@126.com

Received on Jan. 3, 2019

tissue. Thus, a local high-resolution deformation model of soft tissue based on element-free Galerkin method is proposed to simulate the deformation of soft tissue. The model uses an element-free Galerkin method to simulate soft tissue deformation, and applies a uniform streamline method based on octree coding to simplify point data of soft tissue geometric model, meanwhile, integrates Kelvin viscoelastic model and adjustment function to simulate the nonlinear viscoelasticity of soft tissue, so as to improve the real-time and authenticity of soft tissue deformation simulation. In addition, a local high-resolution algorithm is applied to sample and render soft tissue deformation region to provide better visual feedback for users.

1 Methods

Meshless methods use a group of nodes scattered in the problem domain and boundary to represent the problem domain and boundary when establishing an algebraic equation of the whole problem domain system. The method does not need to use the predefined mesh information for domain discretization. The element-free Galerkin method, which is one of the meshless methods, has fast convergence and high efficiency, therefore, this paper applies it to establish soft tissue models and solves corresponding equations.

1.1 Element-free Galerkin method

Since the element-free Galerkin method is easy to implement and the calculation accuracy is high, this paper applies it to define the point cloud of discrete geometry. Assume that a three-dimensional elastomer has volume Ω and boundary surface Γ, as shown in Fig. 1.

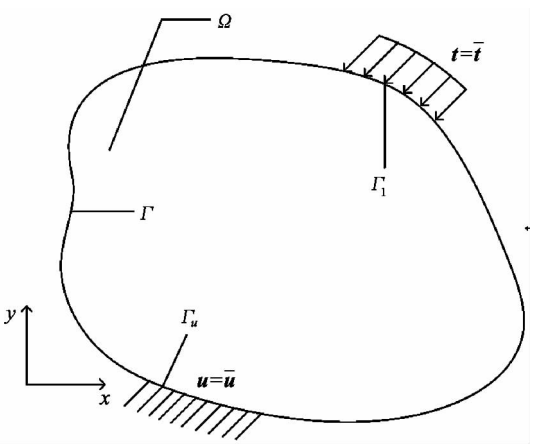

Fig. 1 Schematic diagram of interaction between soft tissue and surgical instruments

The equilibrium equation in Ω is expressed as follows:

$$\boldsymbol{L}\cdot\boldsymbol{\sigma}+\boldsymbol{b}=0 \quad \text{in } \Omega \tag{1}$$

where $\boldsymbol{L}$, $\boldsymbol{\sigma}$ and $\boldsymbol{b}$ are differential operator matrix, stress tensor and physical force vector, respectively.

The relationship between constitutive and strain-displacement is as follows:

$$\boldsymbol{\sigma}=\boldsymbol{D}\boldsymbol{\varepsilon},\ \boldsymbol{\varepsilon}=\boldsymbol{L}^{\mathrm{T}}\boldsymbol{u} \tag{2}$$

where $\boldsymbol{D}$, $\boldsymbol{\varepsilon}$, $\boldsymbol{L}^{\mathrm{T}}$ and $\boldsymbol{u}$ are material elastic matrix, strain vector, transposition of differential operator matrix $\boldsymbol{L}$ and displacement vector, respectively.

Boundary Γ_t and Γ_u define the natural and essential boundary conditions, respectively:

$$\boldsymbol{\sigma}\cdot\boldsymbol{n}=\bar{\boldsymbol{t}} \ \text{ on } \Gamma_t \tag{3}$$

$$\boldsymbol{u}=\bar{\boldsymbol{u}} \ \text{ on } \Gamma_u \tag{4}$$

where $\boldsymbol{n}$, $\bar{\boldsymbol{t}}$ and $\bar{\boldsymbol{u}}$ are the unit vectors which are perpendicular to the boundary surface, the specified surface force and the specified displacement, respectively.

The shape function of the element-free Galerkin method is constructed by moving least squares method, but the moving least squares method does not show the Kronecker $-\delta$ functions property, for establishing Eq. (1) and Eqs(3) – (4), the following constraint Galerkin weak form is used:

$$\int_{\Omega}\delta(\boldsymbol{L}\boldsymbol{u})^{\mathrm{T}}\boldsymbol{D}(\boldsymbol{L}\boldsymbol{u})\,\mathrm{d}\Omega-\int_{\Omega}\delta\boldsymbol{u}^{\mathrm{T}}\boldsymbol{b}\,\mathrm{d}\Omega-\int_{\Gamma_t}\delta\boldsymbol{u}^{\mathrm{T}}\bar{\boldsymbol{t}}\,\mathrm{d}\Gamma-\delta\int_{\Gamma_u}\frac{1}{2}(\boldsymbol{u}-\bar{\boldsymbol{u}})^{\mathrm{T}}\alpha(\boldsymbol{u}-\bar{\boldsymbol{u}})=0 \tag{5}$$

where δ and α represent Kronecker $-\delta$ functions value and penalty factor, respectively.

1.2 Moving least squares method

Moving least squares method has been widely used to construct meshless shape function due to its fast convergence. In the meshless method, since there is no mesh, field variable $\boldsymbol{u}$ at any point $X=(x, y, z)$ in the problem domain needs to use the function value of the field node in the local support domain to approximate, so let $u(X)$ be the field function defined in Ω, and $u^h(X)$ is the approximation of $u(X)$ in position X, where $u(X)$ can be expressed as

$$u(X)\approx u^h(X)=\boldsymbol{P}^{\mathrm{T}}(X)\boldsymbol{a}(X) \tag{6}$$

where, $\boldsymbol{P}^{\mathrm{T}}(X)$ and $\boldsymbol{a}(X)$ represent the polynomial basis function vector and the non-constant coefficient vector, respectively.

In three-dimensional space, the basis function vector is usually composed of a single algebraic term:

$$\boldsymbol{P}^{\mathrm{T}}(X)=[1, x, y, z] \tag{7}$$

By considering the weight function $w_i(X)=w(X-X_i)$ of each node and minimizing the approximation error of Euclidean norm $J(X)$, $\boldsymbol{a}(X)$ can be derived by Eq. (8), shown in Eq. (9):

$$J(X) = \sum_{i=1}^{n} w(X - X_i)(\boldsymbol{P}^{\mathrm{T}}(X_i)\boldsymbol{a}(X) - u_i)^2 \tag{8}$$

$$\boldsymbol{a}(X) = \boldsymbol{A}^{-1}(X)\boldsymbol{C}(X)\boldsymbol{u} \tag{9}$$

where the weighted moment matrix $\boldsymbol{A}(X)$ is defined as

$$\boldsymbol{A}(X) = \boldsymbol{P}^{\mathrm{T}}(X)\boldsymbol{W}(X)\boldsymbol{P}(X) \tag{10}$$

$$\boldsymbol{C}(X) = \boldsymbol{P}^{\mathrm{T}}(\mathrm{X})\boldsymbol{W}(X) \tag{11}$$

where $\boldsymbol{W}(X)$ and $\boldsymbol{P}(X)$ are weight function matrix and polynomial basis function matrix, respectively. And they are defined as follows:

$$\boldsymbol{W}(X) = \begin{bmatrix} w_1(X) & 0 & \cdots & 0 \\ 0 & w_2(X) & \cdots & 0 \\ \vdots & \vdots & \ddots & \vdots \\ 0 & 0 & \cdots & w_n(X) \end{bmatrix} \tag{12}$$

$$\boldsymbol{P}(X) = \begin{bmatrix} \boldsymbol{P}^{\mathrm{T}}(X_1) \\ \boldsymbol{P}^{\mathrm{T}}(X_2) \\ \vdots \\ \boldsymbol{P}^{\mathrm{T}}(X_n) \end{bmatrix} \tag{13}$$

The approximation field function can be expressed as

$$u(X) \approx u^h(X) = \boldsymbol{\Phi}(X)\boldsymbol{u} = \sum_{i=1}^{n} \Phi_i(X)u_i \tag{14}$$

where $\boldsymbol{\Phi}(X)$, $\Phi_i(X)$ and u_i are the shape function, the shape function of node i and the displacement of node i, respectively. $\boldsymbol{\Phi}(X)$ can be defined as

$$\boldsymbol{\Phi}(X) = \boldsymbol{P}^{\mathrm{T}}(X)\boldsymbol{A}^{-1}(X)\boldsymbol{C}(X) \tag{15}$$

where $\boldsymbol{A}^{-1}(X)$ denotes the inverse matrix of the weighted moments matrix $\boldsymbol{A}(X)$.

The weight function plays an important role in the construction of the shape function. In particular, the smoothness of the weight function determines the continuity of the shape function. In the soft tissue modeling, the cubic spline weight function is generally used as the weight function $w(s_i)$.

$$w(s_i) = \begin{cases} \dfrac{2}{3} - 4s_i^2 + 4s_i^3, & s_i \leqslant \dfrac{1}{2} \\ \dfrac{4}{3} - 4s_i + 4s_i^2 - \dfrac{4}{3}s_i^3, & \dfrac{1}{2} < s_i \leqslant 1 \\ 0, & \text{others} \end{cases} \tag{16}$$

where the radius affected by the dimensionless weight function is expressed as $s_i = \dfrac{\| X - X_i \|}{\rho_i}$, ρ_i represents the radius of the range affected by node i.

2 Nonlinear viscoelastic high-resolution meshless model

Real soft tissue has biological viscoelastic characteristics. However, the traditional meshless soft tissue modeling method can not reflect its viscoelasticity, which reduces the virtual soft tissue simulation authenticity. Therefore, the nonlinear viscoelastic model is established and integrated into the element-free Galerkin method. At the same time, in order to show more details of the local deformation region, this paper applies a local high-resolution algorithm for optimization in the post-processing to provide users with better visual feedback and reduce the calculation cost.

2.1 Establishment of nonlinear viscoelastic model

The Kelvin viscoelastic model consists of two springs and a damper, as shown in Fig. 2, where the spring can represent the linear properties of the soft tissue and the damper can represent the damping characteristics of the soft tissue when it is deformed[15]. Therefore, Kelvin viscoelastic model is used to construct soft tissue mechanics model to describe the viscoelastic properties of soft tissue.

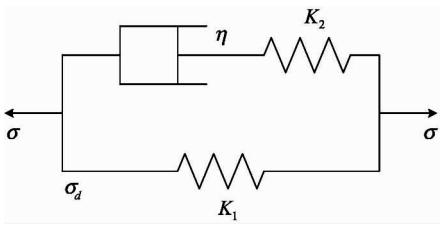

Fig. 2 Kelvin viscoelastic model

In Fig. 2, σ, σ_d, η, K_1 and K_2 represent stress, stress time derivative, damper, the stiffness of the first and second springs in the model, respectively. Because the nonlinear viscoelastic tissue mechanics model can reflect the biological properties of the soft tissue better, and can realize better simulation effect than linear viscoelastic model, therefore, an adjustment function is integrated to the viscoelastic relaxation constitutive relation to show the nonlinear relationship between stress and strain in this paper.

In the Kelvin viscoelastic model, the relaxation constitutive relation of soft tissue under stress can be expressed as

$$\sigma(t) = \int_0^t E(t - \tau)\frac{\mathrm{d}\varepsilon}{\mathrm{d}\tau}\mathrm{d}\tau \tag{17}$$

where $\sigma(t)$, $E(t)$ and ε are the relaxation response, relaxation modulus and strain of the material, respectively.

In order to show the nonlinear relationship between stress and strain, an adjustment function $N(\varepsilon)$ is integrated to the viscoelastic relaxation constitutive relation. The nonlinear viscoelastic relaxation constitutive relation is expressed as follows:

$$\sigma(t) = \int_0^t E(t-\tau)\frac{\mathrm{d}N(\varepsilon)}{\mathrm{d}\tau}\mathrm{d}\tau \tag{18}$$

$$N(\varepsilon) = \varepsilon + k\varepsilon^2 \tag{19}$$

Deformation simulation time T is divided into n time slices t_1, t_2, $\cdots$, t_n. $\Delta t = T/n$ is a time increment. From moment t_n to moment t_{n+1}, Δu_n, $\Delta\sigma_n$ and $\Delta\varepsilon_n$ represent the increment of displacement, stress and strain, respectively. The stress of Kelvin model at moment t_n and moment t_{n+1} is expressed as

$$\sigma_n = \int_0^h E(t_n-\tau)\frac{\mathrm{d}N(\varepsilon)}{\mathrm{d}\tau}\mathrm{d}\tau \tag{20}$$

$$\sigma_{n+1} = \int_0^h E(t_{n+1}-\tau)\frac{\mathrm{d}N(\varepsilon)}{\mathrm{d}\varepsilon}\frac{\mathrm{d}\varepsilon}{\mathrm{d}\tau}\mathrm{d}\tau + \Delta\varepsilon_n\left[\frac{1}{\Delta t}\int_{t_n}^{t_{n+1}} E(t_{n+1}-\tau)\frac{\mathrm{d}N(\varepsilon)}{\mathrm{d}\tau}\mathrm{d}\tau\right] \tag{21}$$

The incremental form of the nonlinear viscoelastic model can be expressed as

$$\Delta\sigma_n = E_k\Delta\varepsilon_n + \sigma_{0,n} \tag{22}$$

where E_k is the nonlinear relaxation coefficient and $\sigma_{0,n}$ represents the initial stress.

At moment t_{n+1}, displacement, stress and strain can be expressed as follows:

$$u_{n+1} = u_n + \Delta u_n \tag{23}$$

$$\sigma_{n+1} = \sigma_n + \Delta\sigma_n \tag{24}$$

$$\varepsilon_{n+1} = \varepsilon_n + \Delta\varepsilon_n \tag{25}$$

The relationship between strain and displacement can be expressed as follows:

$$\varepsilon_{n+1} = \boldsymbol{L}u_{n+1} + \boldsymbol{L}\Delta u_n \tag{26}$$

2.2 Integrate the nonlinear viscoelastic model

By integrating the nonlinear viscoelastic model into the element-free Galerkin method, a meshless solution equation for simulating the nonlinear viscoelastic soft tissue deformation is derived, which can accurately simulate the soft tissue deformation in virtual surgery.

By substituting Eqs(22) – (26) into Eq. (5), the incremental form of nonlinear viscoelastic meshless solution equation can be obtained:

$$[\boldsymbol{K}_n + \boldsymbol{K}_n^{\alpha}]\Delta u_n = \Delta\boldsymbol{R}_n \tag{27}$$

where $\boldsymbol{K}_n$, $\boldsymbol{K}_n^{\alpha}$ and $\Delta\boldsymbol{R}_n$ are the viscoelastic stiffness matrix, the penalty stiffness matrix that is determined by the shape function and the derivative of the shape function in the element-free Galerkin method and unbalanced force vector, respectively. They are defined as follows:

$$\boldsymbol{K}_n = \sum_{\Omega}\int_{\Omega}[\boldsymbol{B}_i^{\mathrm{T}}\boldsymbol{E}_k\boldsymbol{B}_j]\mathrm{d}\Omega \tag{28}$$

where $\boldsymbol{B}_i$ is the matrix of the derivative of the shape function of node i, it is defined as follows:

$$\boldsymbol{B}_i = \begin{bmatrix} \Phi_{i,x} & 0 & 0 \\ 0 & \Phi_{i,y} & 0 \\ 0 & 0 & \Phi_{i,z} \\ \Phi_{i,y} & \Phi_{i,x} & 0 \\ 0 & \Phi_{i,z} & \Phi_{i,y} \\ \Phi_{i,z} & 0 & \Phi_{i,x} \end{bmatrix} \tag{29}$$

where $\Phi_{i,x}$, $\Phi_{i,y}$ and $\Phi_{i,z}$ represent the derivative of the shape function with respect to x, y and z at node i, respectively. In the same way, $\boldsymbol{B}_j$ can be gotten.

$$\boldsymbol{K}_n^a = \sum_{\Gamma}\int_{\Gamma}[\Phi_i^{\mathrm{T}}a\Phi_j]\mathrm{d}\Gamma \tag{30}$$

$$\Delta\boldsymbol{R}_n = \sum -\int_{\Omega}\delta(\Delta\varepsilon_n)^{\mathrm{T}}\sigma_n\mathrm{d}\Omega - \int_{\Omega}\delta(\Delta\varepsilon_n)^{\mathrm{T}}\sigma_{0,n}\mathrm{d}\Omega + \int_{\Omega}\delta(\Delta u_n)^{\mathrm{T}}\mathrm{b}\boldsymbol{d}\Omega - \int_{\Gamma_t}\delta(\Delta u_n)^{\mathrm{T}}\bar{t}_n\mathrm{d}\Gamma + \delta\int_{\Gamma_u}\frac{1}{2}(\Delta u_n - \Delta\bar{u})^{\mathrm{T}}a(\Delta u_n - \Delta\bar{u})\mathrm{d}\Gamma \tag{31}$$

Given the corresponding material parameters and time step, it can be calculated according to Eq. (27) to calculate Δu_n and calculate the new displacement, stress and strain at each point.

2.3 Optimization of local high-resolution algorithm

According to the survey, the human visual system is more sensitive to the rendering effect of deformed region than non-deformed region[16]. In order to provide users with more rendering feedback details of soft tissue deformation, a local high-resolution algorithm is applied to select a certain sample points in the deformed region and render them. The points can be selected densely near the surgical instrument, there by reducing the calculation cost and not affecting the simulation authenticity in this method.

The detailed process is as follows: First, point cloud data is collected from the region where the soft tissue is applied by the surgical instrument. Then, calculate l the nearest surface points of each point in the sampling points, so as to obtain the set $N_u(d_i)$ of l the nearest points of all the non-sampled surface points d_i and a set $N_s(d_i)$ of l the nearest points in all volume data including surface and internal sampling points d_i, in which $d_i \in D_s$ and D_s represents the point set of the applied force region. Fig. 3 is the schematic diagram of the surface neighboring points set.

In each time step, the nonlinear viscoelastic meshless solution equation described in section 2.2 is used to calculate the new position of each point. According to $N_s(d_i)$, the affine transformation matrix of d_i

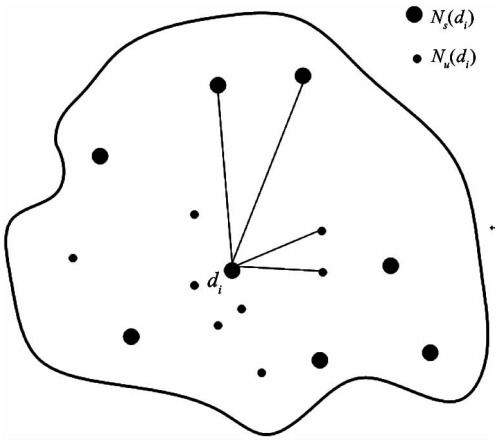

Fig. 3 Schematic diagram of surface neighboring points set

is obtained from the initial position and current position of each point, and it is used to calculate the new position of each point that belongs to $N_u(d_i)$ and then the region is rendered.

3 Implementation and results

In order to verify the proposed model, the soft tissue simulation is implemented by using the model. The algorithm flowchart of the model is shown in Fig. 4.

First, CT images are imported into software Mimics. Then, a 3D model is generated. After the STL file is derived, convert OBJ files by MeshLab to get point cloud data. The uniform streamline method based on octree coding is applied to simplify the data. After that, element-free Galerkin method is applied to define the cloud of nodes, and by the moving least squares method based on the nodes of the local domain, the shape function, an approximate field function described in the form of node variables is defined.

On the basis of the above, Kelvin viscoelastic model and adjustment function are integrated. The shape function and the weak system equation are integrated to form the discrete system equation of the meshless method, and the displacement caused by stress deformation in the displacement field is obtained by solving the discrete system equation of the meshless method. Finally, the model is post-processed using the local high-resolution optimization algorithm.

The specific details of the experiments and the verification of the model performances are described in detail in the following subsections.

3.1 Data acquisition and simplification

In this paper, the meshless method is adopted for modeling, and point cloud data is essential. The CT image of soft tissue is imported into the Mimics software

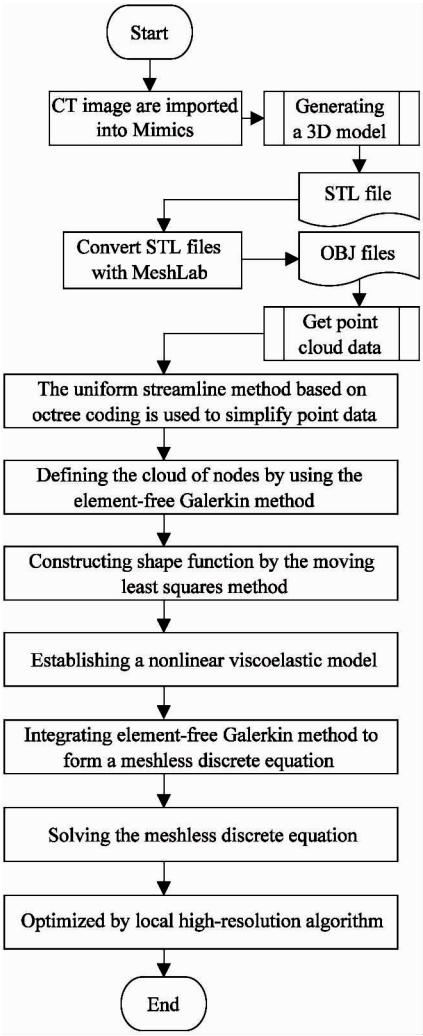

Fig. 4 Algorithm flowchart

to generate 3D images and then the 3D model STL file is exported. The software MeshLab is used to convert the STL file into OBJ file to obtain the vertex information and get the point cloud data.

The geometric model generated from Mimics contains a large amount of data, which consumes a lot of time during the implementation. In order to improve the real-time performance of virtual surgery, the uniform streamline method based on octree coding is adopted to simplify point data. The method divides the point cloud data space into several cubes with fixed edge length, keeps the closest center point of each cube, calculates the octree coding of each point, recovers points from small to large. Points with same coding value are stored in a same chain table. The method only selects the point that is the closest to the center point if there are multiple points in the same chain table, so as to simplify the process.

3.2 Experimental environment

VC ++ 2017, 3D Max and OpenGL are used, and CHAI3D open-source software package is used to provide force feedback API to drive the tactile interface. The system hardware includes a computer with Intel Core i9-7960x CPU and NVIDIA GeForce 1080Ti, and Sensable Phantom Omniforce tactile device. Fig. 5 shows the simulation environment.

Fig. 5 The simulation environment

3.3 Parameter selection and rendering

To achieve the effectiveness and authenticity of the proposed model in term of visual effects, the method mentioned in section 3.1 is used to obtain the liver point cloud data. The liver model with 3 980 data points is constructed, using surgical instruments applied respectively 1.0 N, 1.5 N, 2.0 N deformation stress and tension and observe the results. As shown in Fig. 6 and Fig. 7, different external forces are applied on the liver, and the deformation effect is realistic. In the interactive process of using surgical instruments to press and stretch, the soft tissue operability and deformation authenticity requirements are met.

3.4 Correctness verification

In order to verify the correctness of the proposed model, the liver model established in this paper is compared with creep response data in Ref. [17]. In Fig. 8, the curve with vertical squares and the curve with regular squares represent the deformation and displacement curves of the top and bottom of the ex vivo pig liver under 1.0 N external force respectively, while the curve with stars represents the deformation and displacement curves of the proposed model. The experimental results show that displacement curves of the proposed model and actual liver have same variation trend in the deformation, so the deformation of the proposed model is effective and nonlinear.

3.5 Visual validation

In order to show more details of the model in the local deformation region, point-based model[18], interpolation model[19] and the proposed model are adopted and based on these three models, the brain tumor is modeled and deformed by external forces. The magnification diagrams of local deformation that are generated based on the three above models under the same pressure are shown respectively in Fig. 9. The local deformation magnification diagrams that are generated based

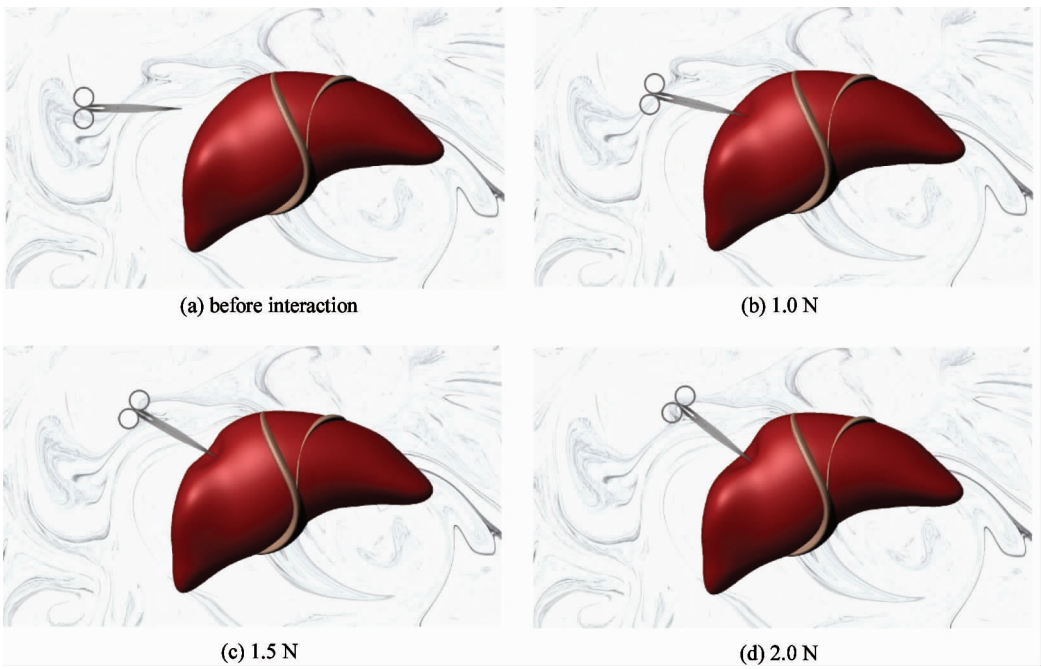

Fig. 6 Rendering effect of liver deformation under different pressures

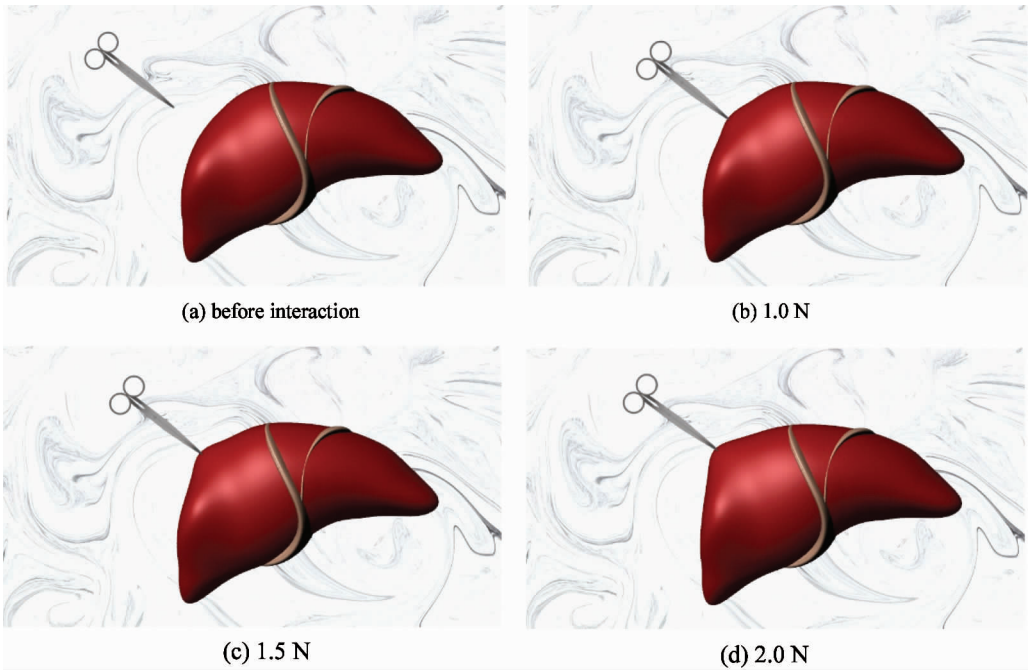

Fig. 7 Rendering effect of liver deformation under different tensions

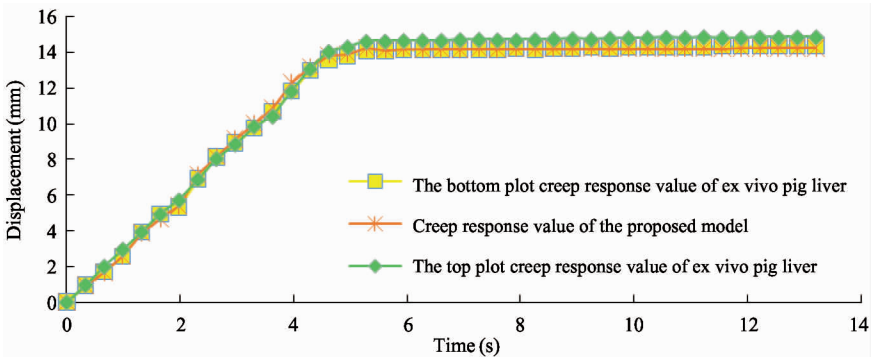

Fig. 8 Comparison of creep response under 1.0N external force

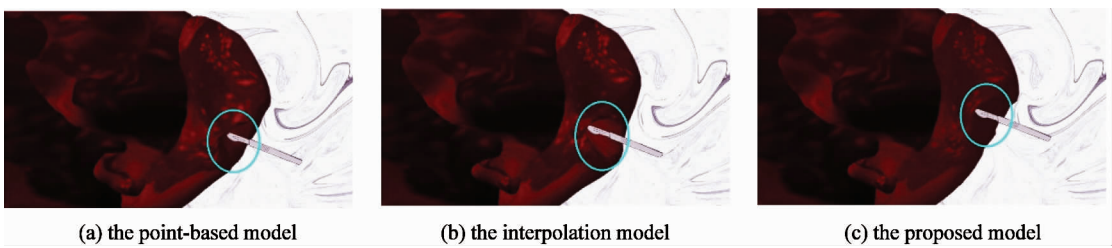

Fig. 9 Magnification of local deformation under the same pressure

on the three above models under the same tension respectively are shown in Fig. 10. It can be seen that the local deformation surface of brain tumor constructed based on the point model is rough and distorted, the interpolation model renders the local deformation surface with good deformation effect, and the local deformation surface of the proposed model has the most abundant and smooth details.

3.6 Computational efficiency verification

To verify the computational efficiency of the proposed model, four different numbers of sample points are selected, and the point-based model[18], the interpolation model[19] and the proposed model are used. As shown in Table 1, when the number of points increases, the execution time per time step and the surface rendering time of each model increases continuously.

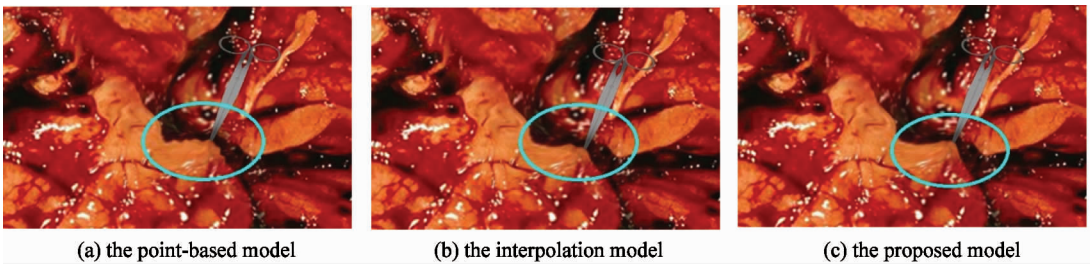

(a) the point-based model (b) the interpolation model (c) the proposed model

Fig. 10 Magnification of local deformation under the same tensile force

Table 1 Calculation time of different quantity points

No	Number of sample points	Execution time per time step(ms) (the point-based model)	Execution time per time step(ms) (the interpolation model)	Execution time per time step(ms) (the proposed model)	Surface render time(ms) (the point-based model)	Surface render time(ms) (the interpolation model)	Surface render time(ms) (the proposed model)
1	89	3.51	4.75	2.55	0.011	0.012	0.008
2	185	6.85	9.22	4.87	0.067	0.072	0.049
3	1604	76.92	73.44	39.77	0.693	0.756	0.449
4	3236	164.53	157.23	75.10	2.891	2.723	1.606

At the same time, as shown in Fig. 11 and Fig. 12, when the number of points is same, the execution time per time step and the surface rendering time consumed by the proposed model is less than that of other models, indicating that the proposed model has better real-time performance.

3.7 Comparison of comprehensive evaluation

To verify the comprehensive performance of the proposed model, visual fluency, force feedback performance, immersion and system stability are chosen and these four commonly used evaluation indexes are denoted by 1, 2, 3 and 4, respectively. Using the sorting method of approximate ideal solution, the proposed model is compared with the point-based model, mass-spring model and finite element model.

Twenty-eight physicians work in First Affiliated Hospital of Nanjing Medical University are randomly invited, including 4 chief physicians marked Y_1, 7 deputy chief physicians marked Y_2, 10 attending physicians marked Y_3 and 7 interns marked Y_4. The score weights of the four kinds of physicians are 0.35, 0.3,

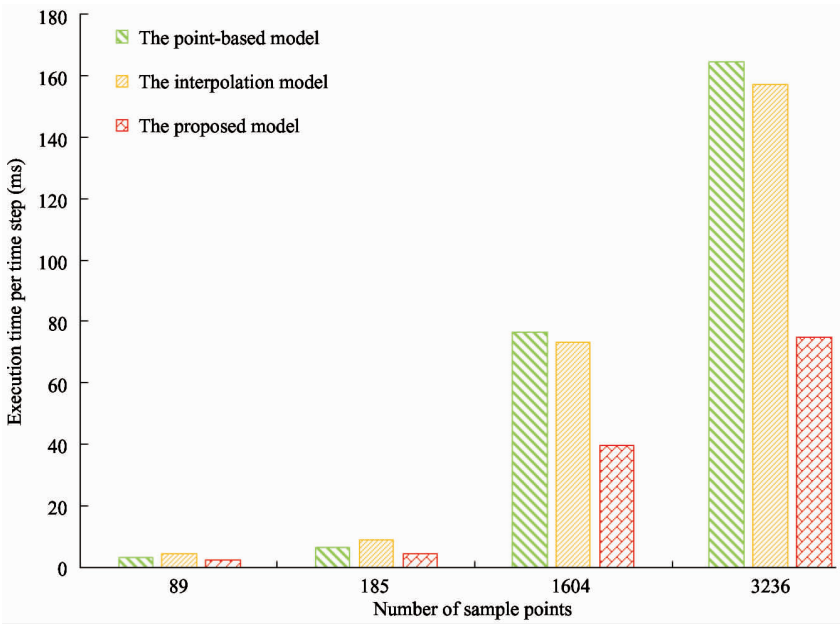

Fig. 11 Execution time per time step for different sample points

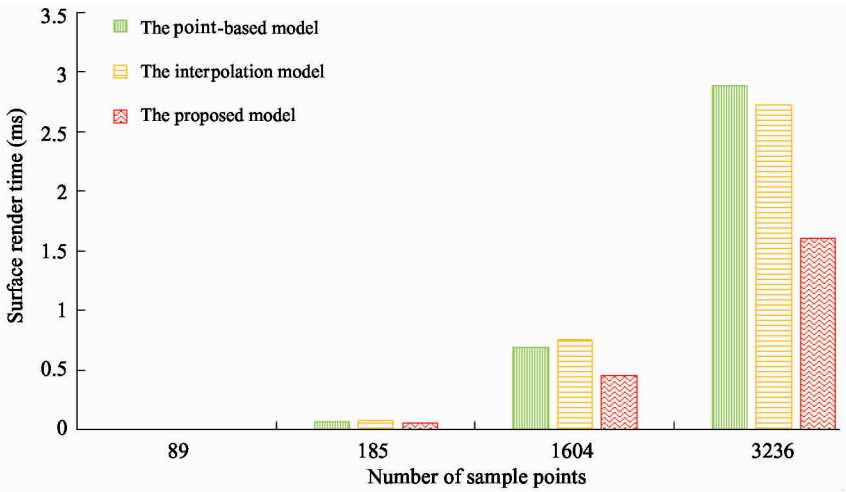

Fig. 12 Surface rendering time for different sample points

0.25 and 0.1, respectively. 28 physicians interacted with liver models built by four models via the Sensable Phantom Omni and scored each model on a scale of 0 to 10. The index scores $f_{ij}(i = 1,2,3,4, j = 1,2,3,4)$ of the four models are calculated by

$$f_{ij} = 35\% \cdot \left(\sum_{i=1}^{4} Y_{1i}/4\right) + 30\% \cdot \left(\sum_{i=1}^{7} Y_{2i}/7\right) + 25\% \cdot \left(\sum_{i=1}^{10} Y_{3i}/10\right) + 10\% \cdot \left(\sum_{i=1}^{7} Y_{4i}/7\right) \tag{32}$$

The four index scores $f_{ij}(i = 1,2,3,4, j = 1,2,3,4)$ of the four models can form a decision matrix $\boldsymbol{A}$.

$$\boldsymbol{A} = \begin{bmatrix} f_{11} & f_{12} & f_{13} & f_{14} \\ f_{21} & f_{22} & f_{23} & f_{24} \\ f_{31} & f_{32} & f_{33} & f_{34} \\ f_{41} & f_{42} & f_{43} & f_{44} \end{bmatrix} \tag{33}$$

Normalized decision matrix $\boldsymbol{Z}$ can be composed of a decision matrix $\boldsymbol{A}$, whose elements are $Z_{ij}(i = 1,2,3,4, j = 1,2,3,4)$:

$$Z_{ij} = \frac{f_{ij}}{\sqrt{\sum_{i=1}^{4} f_{ij}^2}} \quad i = 1,2,3,4, j = 1,2,3,4 \tag{34}$$

The larger the element value Z_{ij} in the normalized decision matrix $\boldsymbol{Z}$ is, the better the index is. Therefore, the ideal solution set Z^+ and negative ideal solution set Z^- of each column are determined as follows:

$$Z^+ = (Z_1^+, Z_2^+, Z_3^+, Z_4^+) = \{\max_i Z_{ij} \mid j = 1,2,3,4\} \tag{35}$$

$$Z^- = (Z_1^-, Z_2^-, Z_3^-, Z_4^-) = \{\min_i Z_{ij} \mid j = 1,2,3,4\} \tag{36}$$

The distance D_i^+ between each model index value and the ideal point and the distance D_i^- between each model index value and the negative ideal point is calculated as

$$D_i^+ = \sqrt{\sum_{j=1}^{4} (Z_{ij} - Z_j^+)^2} \quad i = 1,2,3,4 \tag{37}$$

$$D_i^- = \sqrt{\sum_{j=1}^{4} (Z_{ij} - Z_j^-)^2} \quad i = 1,2,3,4 \tag{38}$$

Finally, Eq. (39) is used to calculate the relative approximation C_i of each model index value to the ideal solution.

$$C_i = \frac{D_i^-}{D_i^- + D_i^+} \quad 0 \leqslant C_i \leqslant 1, \ i = 1,2,3,4 \tag{39}$$

Table 2 shows the index values and sorting results of relative approximations compared to optimal values of different models. It can be seen from Table 2 that the comprehensive evaluation of the proposed model is the closest to the optimal value, thus the comprehensive superiority of the proposed model is verified.

Table 2 Index values and sorting results of relative approximations compared with optimal values of different models

Model type	$D+$	$D-$	Ci	Sorting result
The proposed model	0.017	0.048	0.738	1
The point-based model	0.029	0.028	0.491	3
Mass-spring model	0.053	0.000	0.000	4
Finite element model	0.024	0.039	0.619	2

4 Conclusion

Based on viscoelastic mechanics, a local high-resolution deformation model of soft tissue based on element-free Galerkin method is proposed to simulate soft tissue deformation in virtual surgery. This model applies the high accuracy and stability element-free Galerk-in method to calculate the process of soft tissue deformation. Since it only needs point information, the proposed model is suitable for simulating complex topological changes in soft tissue. In addition, the geometric model of soft tissue is simplified before calculation, so calculation cost is reduced. Due to the integration of Kelvin viscoelastic model and adjustment function, and the application of the local high-resolution algorithm, the simulation authenticity and visual feedback quality are improved. Liver and brain tumor deformation simulation experiments were performed on the Sensable Phantom Omni force tactile interaction device, and the proposed model was compared with other meshless models. The experimental results show that the simulation accuracy and computational efficiency of this model are higher, the visual feedback is better, and the comprehensive advantages in terms of visual fluency, force feedback performance, immersion and system stability are obvious.

References

[1] Zhang X R, Zhu J D, Sun W, et al. Virtual brain surgery simulation system based on haptic interaction[J]. *High Technology Letters*, 2015, 21(2): 185-191

[2] Zou Y N, Liu P X. A new deformation simulation algorithm for elastic-plastic objects based on splat primitives [J]. *Computers in Biology & Medicine*, 2017, 83:84-93

[3] Cheng Q Q, Liu P X, Lai P H, et al. An interactive meshless cutting model for nonlinear viscoelastic soft tissue in surgical simulators[J]. *IEEE Access*, 2017, 5: 16359-16371

[4] Zou Y N, Liu P X. A high-resolution model for soft tissue deformation based on point primitives[J]. *Computer Methods & Programs in Biomedicine*, 2017, 148:113-121

[5] Zhang X R, Duan J L, Zhu L F, et al. A virtual puncture surgery system based on multi-layer soft tissue and force mesh[J]. *Computers Materials & Continua*, 2018, 57(3): 505-519

[6] Li C, Ding J, Hong Z, et al. A surface mass-spring model with new flexion springs and collision detection algorithms based on volume structure for real-time soft-tissue deformation interaction [J]. *IEEE Access*, 2018, 6: 75572-75597

[7] Zhang X R, Wang P P, Sun W, et al. The torsion model of soft tissue in virtual surgery[J]. *High Technology Letters*, 2018, 24(2): 169-179

[8] Liu X, Yao J. Modelling and simulation of vascular tissue based on finite element method[C]. In: 2018 5th International Conference on Information Science and Control Engineering, Zhengzhou, China, 2018. 336-340

[9] Noël C. A three-dimensional visco-hyperelastic FE model for simulating the mechanical dynamic response of preloaded phalanges[J]. *Medical Engineering & Physics*, 2018, 61: 41-50

[10] Yin S F, Xue S L, Li B, et al. Bio-chemo-mechanical modeling of growing biological tissues: finite element method[J]. *International Journal of Non-Linear Mechanics*, 2019, 108: 46-54

[11] Dong Y, Liu X, Li H, et al. A nonlinear viscoelastic meshless model for soft tissue deformation[C]. In: 2016 International Conference on Virtual Reality and Visualization, Hangzhou, China, 2016. 204-211

[12] Cheng Q Q, Liu P X, Lai P H, et al. A novel haptic interactive approach to simulation of surgery cutting based on mesh and meshless models[J]. *Journal of Healthcare Engineering*, 2018, 2018: 1-16

[13] Zhou J, Liu X, Li C. A meshless deformation simulation method for virtual surgery[J]. *International Journal of Robotics and Automation*, 2018, 33(2): 118-126

[14] Zhou J, Luo Z, Li C, et al. Real-time deformation of human soft tissues: aradial basis meshless 3D model based on Marquardt's algorithm[J]. *Computer Methods and Programs in Biomedicine*, 2018, 153: 237-252

[15] Zou Y N, Liu P X, Cheng Q Q, et al. A new deformation model of biological tissue for surgery simulation [J]. *IEEE Transactions on Cybernetics*, 2017, 47(11): 3494-3503

[16] Cheng M M, Mitra N J, Huang X, et al. Global contrast based salient region detection[J]. *IEEE Transactions on Pattern Analysis and Machine Intelligence*, 2014, 37(3): 569-582

[17] Kerdok A E, Ottensmeyer M P, Howe R D. Effects of perfusion on the viscoelastic characteristics of liver[J]. *Journal of Biomechanics*, 2006, 39(12): 2221-2231

[18] Dehghan M, Narimani N. An element-free Galerkin meshless method for simulating the behavior of cancer cell invasion of surrounding tissue[J]. *Applied Mathematical Modelling*, 2018, 59: 500-513

[19] Shivanian E, Jafarabadi A. Capillary formation in tumor angiogenesis through meshless weak and strong local radial point interpolation[J]. *Engineering with Computers*, 2018, 34(3): 603-619

Zhang Xiaorui, born in 1979. She received her Ph. D degree in Instrument Science and Technology Department of Southeast University in 2010. She also received her B. S. and M. S. degrees from Henan University of Science and Technology in 2004 and 2007 respectively. Her research interests include the virtual reality, human-computer interaction, and image processing.